Numerical investigation on W-type index Chalcogenide fiber based MIR supercontinuum generation

M. A. Khamis[a,b], R. Sevilla[a] and K. Ennser[a]
[a]College of Engineering, Swansea University, United Kingdom; [b]Baqubah Technical Institute, Middle Technical University, Bagdad, Iraq.

ABSTRACT

This work presents a numerical study of a W-type index chalcogenide fiber design for Mid-Infrared (MIR) supercontinuum (SC) generation beyond 10µm. Our fiber design consists of a $Ge_{15}Sb_{15}Se_{70}$ glass core, a $Ge_{20}Se_{80}$ glass inner cladding and a $Ge_{20}Sb_5Se_{75}$ glass outer cladding. These chalcogenide materials have the advantages to broaden the spectrum to 12µm, due to their low material absorption. The optical mode distribution of the chalcogenide fiber is simulated by a finite element method based on edge elements. With a 6 µm core diameter and a 12 µm inner cladding diameter, the proposed fiber design exhibits flat anomalous dispersion in the wavelength range (4.3-6.5µm), with a peak of about 7ps/(nm.km). The position of the second zero-dispersion wavelength (ZDW) can be easily and precisely controlled by the inner cladding size and should be shifted to around 7µm for a 18 µm inner cladding diameter. This design is more suitable for a pump wavelength at 6.3µm which is in the anomalous dispersion regime between two ZDWs and can broaden the spectrum due to the soliton dynamics. Our fiber design modelling shows that the nonlinear parameter at 6.3µm is $0.1225 W^{-1} m^{-1}$, when using a nonlinear refractive index $n_{NL}=3.44 \times 10^{-18} m^2 W^{-1}$, and the chromatic dispersion is D = 3.24ps/(nm.km). Compared to previously reported step-index fibers, the proposed W-type index chalcogenide structure ensures single mode propagation, which improves the nonlinearity, flattened dispersion profile and reduces the losses, due to a tight confinement of the mode within the core.
Keywords: Nonlinear optical materials, W-type index fiber, Finite element method, Supercontinuum generation.

1. INTRODUCTION

High-power single-mode fiber-based supercontinuum (SC) sources with extremely wide wavelength coverage are a key enabling technology for various applications such as spectroscopy[1] and metrology[2] as well as defense applications[3]. To realize highly coherent Mid-Infrared (MIR) SC generation, there are two important factors[4], a small absolute value of the chromatic dispersion in the MIR region and a small effective mode diameter to increase the nonlinearity. Step-index fibers (SIFs) possess the advantage of higher optical damage threshold, good mechanical robustness and stability against contamination from the ambient environment such as water vapor[5]. In addition, SIFs are easier to splice, cleave and mount when compared to other optical fibers such as photonic crystal fibers (PCFs). These characteristics make the SIF a promising key component in fiber lasers and amplifiers as well as in SC generation sources. However, tailoring the fiber dispersion properties of standard SIFs is a challenging task. Furthermore, SIFs present a weaker nonlinearity compared to a PCF due to larger core diameters and looser confinement of the mode within the core, induced by the reduced contrast of the core-cladding index[6].

One approach to control the chromatic dispersion is by applying a W-type index fiber profile[7,8]. The main advantages of W-type index fibers are the tight light confinement within the fiber core and the flattened dispersion profile, offering more flexibility than SIFs to tailor the fiber dispersion properties, but without the complexity of photonic crystal fibers (PCFs). In addition, the W-type index fibers produce a good control of the locations of zero-dispersion wavelengths (ZDWs) and a large V-parameter value (V = 3.8) under the single-mode operation, allowing larger core diameters compared to SIFs. Furthermore, this fiber type is suitable for all-fiber system because it can be fusion spliced to standard SIF.

Our proposed fiber has $Ge_{15}Sb_{15}Se_{70}$ core glass, $Ge_{20}Se_{80}$ glass inner cladding and $Ge_{20}Sb_5Se_{75}$ glass outer cladding. These materials have relatively large third-order nonlinear refractive index (n_{NL}) and relatively high laser damage threshold, as well as good transmittance in the 2–12 µm region[9,10]. Finite Element Method (FEM) based edge element analysis is applied to calculate the effective index and the chromatic dispersion. This approach eliminates the disadvantages of the scalar

finite element approach of having undesired spurious modes or non-physical solutions and facilitates the implementation of boundary conditions at material interfaces[11].

The calculation of V-parameter for W-type index fiber shows that 6 μm is the optimum core diameter to keep the fiber in the single mode boundary at a large range (4.5-12μm). Our fiber design shifts the zero-chromatic dispersion to longer wavelengths with a smaller core diameter size than in the case of SIF and therefore it enhances the fiber nonlinearity due to a smaller effective area. The proposed chalcogenide fiber design has the potential to realize the highly coherent MIR SC generation beyond 10μm**.**

2. FEM FORMULATION

FEM based edge elements is employed to compute the effective index of the proposed W-type fiber. Contrary to other FEMs, the edge elements considered here lead to spurious-free solutions and a natural imposition of the boundary conditions at material interfaces. We use the vector FEM approach that provide immunity from having spurious modes. The propagation of electromagnetic waves is governed by Maxwell's equations. We start our consideration from the curl Maxwell's equations[12]

$$\nabla\times\mathbf{E}=-j\omega\mu\mathbf{H} \tag{1}$$

$$\nabla\times\mathbf{H}=+j\omega\tilde{\varepsilon}\mathbf{E} \tag{2}$$

Where $\tilde{\varepsilon}=\varepsilon+\sigma/(j\omega)$, σ and ε are the conductivity and the permittivity of dielectric materials. The vector FEM formulation can be shown by using either the magnetic field **H** or electric field **E** (The letters in bold are referred to vector quantities**)**. In our investigation, we take the case of **E** field as that it is nearly the same for **H** field[11]. Taking the curl of Eq. (2) and substituting it in Eq. (1), leads the vector Helmholtz equation:

$$\nabla\times\left(\frac{1}{\mu_r}\nabla\times\mathbf{E}\right)=+k_0^2\varepsilon_r\mathbf{E} \tag{3}$$

Where $\mu_r=\mu/\mu_0$, and k_0 is the free-space wave number which is written as

$$k_0^2=\omega^2\mu_0\varepsilon_0 \tag{4}$$

We assume the dependence of field components on the z coordinate on the form $\exp(-\gamma z)$, the complex propagation (γ) is written as $\gamma=\alpha+j\beta$. The electric field is split into two parts, longitudinal (E_z) and transverse ($\mathbf{E_t}$) components, yielding:

$$\mathbf{E}(x,y,z)=\mathbf{E}(x,y)e^{-\gamma z}=\left[\mathbf{E}_t(x,y)+\hat{z}E_z(x,y)\right]e^{-\gamma z} \tag{5}$$

Now, we decouple the vector Helmholtz of Eq. (3) into transverse and longitudinal components:

$$\nabla_t\times\left(\frac{1}{\mu_r}\nabla_t\times\mathbf{E}_t\right)+\frac{1}{\mu_r}\left(\gamma^2\nabla_t E_z+\gamma^2\mathbf{E}_t\right)=k_o^2\varepsilon_r\mathbf{E}_t \tag{6}$$

$$-\frac{1}{\mu_r}\left(\nabla_t\cdot\left(\nabla_t E_z+\mathbf{E}_t\right)\right)=k_o^2\varepsilon_r E_z \tag{7}$$

The problem is solved on a two-dimensional domain that results of enclosing the structure of interest by an electric wall. The edge element finite element formulation is next derived. First, we multiply Eq. (6) and Eq. (7) by the testing functions $\mathbf{T}_t$ and T_z, respectively and then integrate over the structure Γ which yields to[13]

$$\iint_{\Gamma}\left[\mathbf{T}_t\cdot\nabla_t\times\left(\frac{1}{\mu_r}\nabla_t\times\mathbf{E}_t\right)+\frac{\gamma^2}{\mu_r}\left(\mathbf{T}_t\cdot\nabla_t\mathrm{E}_z+\mathbf{T}_t\cdot\mathbf{E}_t\right)\right]\,ds=k_0^2\varepsilon_r\iint_{\Gamma}\mathbf{T}_t\cdot\mathbf{E}_t ds \tag{8}$$

$$-\frac{1}{\mu_r}\iint_{\Gamma}\mathrm{T}_z\left[\nabla_t\cdot\left(\nabla_t\mathrm{E}_z+\mathbf{E}_t\right)\right]\,ds=k_0^2\varepsilon_r\iint_{\Gamma}\mathrm{T}_z\mathrm{E}_z ds \tag{9}$$

The weak form of the above equation can be written by using the vector identities

$$\begin{aligned}&\frac{1}{\mu_r}\iint_{\Gamma}\left[\left(\nabla_t\cdot\mathbf{T}_t\right)\cdot\left(\nabla_t\times\mathbf{E}_t\right)+\left(\gamma^2\mathbf{T}_t\cdot\nabla\mathrm{E}_z+\gamma^2\mathbf{T}_t\cdot\mathbf{E}_t\right)\right]\,ds\\&=k_0^2\varepsilon_r\iint_{\Gamma}\mathbf{T}_t\cdot\mathbf{E}_t ds-\frac{1}{\mu_r}\int_{d\Gamma}\mathbf{T}_t\cdot\left(\hat{n}\times\nabla\times\mathbf{E}_t\right)dl\end{aligned} \tag{10}$$

$$-\frac{1}{\mu_r}\iint_{\Gamma}\left(\nabla_t\mathrm{T}_z\cdot\nabla_t\mathrm{E}_z+\nabla_t\mathrm{T}_z\cdot\mathbf{E}_t\right)\,ds=k_0^2\varepsilon_r\iint_{\Gamma}\mathrm{T}_z\mathrm{E}_z ds+\frac{1}{\mu_r}\int_{d\Gamma}\left(\mathrm{T}_z\frac{\partial\mathrm{E}_z}{\partial n}+\mathrm{T}_z\hat{n}\cdot\mathbf{E}_t\right)dl \tag{11}$$

We consider the following boundary conditions at the electric wall Γ_1 and the magnetic wall Γ_2[11]

$$\begin{aligned}&\left.\begin{aligned}&\hat{n}\times\mathbf{E}_t=0\\&E_z=0\end{aligned}\right\}on\,\Gamma_1\\&\left.\begin{aligned}&\left(\nabla_t E_z+\mathbf{E}_t\right).\hat{n}=0\\&\nabla_t\times\mathbf{E}_t\quad\quad=0\end{aligned}\right\}on\,\Gamma_2\end{aligned} \tag{12}$$

Then rearranging Eqs (10) and (11) and multiplying Eq. (11) with γ, leads to

$$\frac{1}{\mu_r}\iint_{\Gamma}\left(\nabla_t\cdot\mathbf{T}_t\right)\cdot\left(\nabla_t\times\mathbf{E}_t\right)ds-k_0^2\varepsilon_r\iint_{\Gamma}\mathbf{T}_t\cdot\mathbf{E}_t ds=-\frac{\gamma^2}{\mu_r}\left(\iint_{\Gamma}\mathbf{T}_t\cdot\nabla\mathrm{E}_z ds+\iint_{\Gamma}\mathbf{T}_t\cdot\mathbf{E}_t\,ds\right) \tag{13}$$

$$\frac{\gamma^2}{\mu_r}\iint_{\Gamma}\nabla_t\mathrm{T}_z\cdot\nabla_t\mathrm{E}_z\,ds+\frac{\gamma^2}{\mu_r}\iint_{\Gamma}\nabla_t\mathrm{T}_z\cdot\mathbf{E}_t\,ds=k_0^2\gamma^2\varepsilon_r\iint_{\Gamma}\mathrm{T}_z\mathrm{E}_z ds \tag{14}$$

We use nodal-based elements, as shown in Figure 1(a), and the vector-based tangential edge elements, as shown in Figure 1(b), to approximate the longitudinal component and the transverse fields of the Helmholtz equation Eq. (6) and Eq. (7), respectively[11].

For a single triangular element, we can express the transverse electric field as a superposition of edge elements. The edge elements allow a nonzero tangential component of the basis function along one edge and zero tangential component along the other. We can compute the complete transverse electric field of each triangular element as[11]

$$\mathbf{E}_t=\sum_{m=1}^{3}e_{tm}\mathbf{W}_{tm} \tag{15}$$

Where the indication m is the m-th edge of the triangle and $\mathbf{W}_{tm}$ refers to the vectorial edge element for the edge m which is described by

$$\mathbf{W}_{tm}=L_{tm}\left(\alpha_i\nabla_t\alpha_j-\alpha_j\nabla_t\alpha_i\right) \tag{16}$$

Where L_{tm} indicates the length of the edge m which is connecting the nodes i and j, and α_i is referred to the nodal shape function written by

$$\alpha_i = \frac{1}{2\mathrm{A}}\left(a_i + b_i x + c_i y\right) \tag{17}$$

Where A is the triangle element area, a_i, b_i, and c_i are written by[11]

$$a_i = x_j y_k - x_k y_j \,, b_i = y_j - y_k \,, c_i = x_k - x_j \tag{18}$$

Here *i*, *j*, and *k* are cyclical, and therefore we can write the longitudinal component as

$$\mathrm{E}_z = \sum_{i=1}^{3} e_{zi}\alpha_i \tag{19}$$

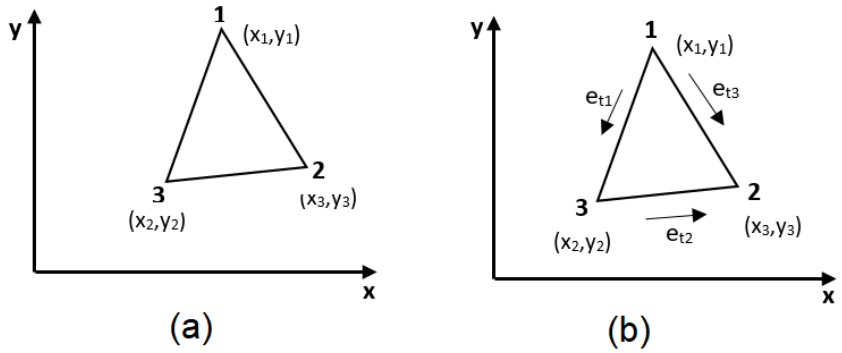

Figure 1. Configuration of (a) node elements and (b) tangential edge elements

We choose the testing function $\mathbf{T}_t$ and T_z corresponding to the vectorial and nodal shape functions, respectively ($\mathbf{T}_t$=$\mathbf{W}_{tm}$ and T_z=α_i), we substitute Eq. (15) and Eq. (19) into Eq. (13) and Eq. (14), integrates over a single element and interchange the integration and summation yields to[11]

$$\begin{aligned} &\frac{1}{\mu_r}\sum_{m=1}^{3}\iint_{\Delta}\left(\nabla_t \times \mathbf{W}_{tm}\right)\cdot\left(\nabla_t \times \mathbf{W}_{tn}\right)e_{tm}\,ds - k_0^2\sum_{m=1}^{3}\varepsilon_r\iint_{\Delta}\left(\mathbf{W}_{tm}\cdot\mathbf{W}_{tn}\right)e_{tm}\,ds \\ &= -\gamma^2\left[\frac{1}{\mu_r}\sum_{m=1}^{3}\iint_{\Delta}\left(\mathbf{W}_{tm}\cdot\nabla\alpha_j\right)e_{zj}\,ds + \frac{1}{\mu_r}\sum_{m=1}^{3}\iint_{\Delta}\left(\mathbf{W}_{tm}\cdot\mathbf{W}_{tn}\right)e_{tm}\,ds\right] \end{aligned} \tag{20}$$

$$\frac{\gamma^2}{\mu_r}\sum_{i=1}^{3}\iint_{\Delta}\left(\nabla\alpha_i\cdot\nabla\alpha_j\right)e_{zi}\,ds + \frac{\gamma^2}{\mu_r}\sum_{i=1}^{3}\iint_{\Delta}\left(\nabla\alpha_i\cdot\mathbf{W}_{tn}\right)e_{tn}\,ds = \gamma^2\sum_{i=1}^{3}k_0^2\varepsilon_r\iint_{\Delta}\alpha_i\alpha_j e_{zi}\,ds \tag{21}$$

Where n and j =1, 2, 3. We can write Eq. (20) and Eq. (21) as a matrix formation as:

$$\begin{bmatrix} S_{e(tt)} & 0 \\ 0 & 0 \end{bmatrix}\begin{bmatrix} e_t \\ e_z \end{bmatrix} = -\gamma^2\begin{bmatrix} \mathrm{T}_{e(tt)} & \mathrm{T}_{e(tz)} \\ \mathrm{T}_{e(zt)} & \mathrm{T}_{e(zz)} \end{bmatrix}\begin{bmatrix} e_t \\ e_z \end{bmatrix} \tag{22}$$

The matrix elements are as follows:

$$S_{e(tt)} = \frac{1}{\mu_r}\iint_{\Delta}\left(\nabla_t \times \mathbf{W}_{tm}\right)\cdot\left(\nabla_t \times \mathbf{W}_{tn}\right)ds - k_0^2\varepsilon_r\iint_{\Delta}\left(\mathbf{W}_{tm}\cdot\mathbf{W}_{tn}\right)ds \tag{23}$$

$$\mathrm{T}_{e(tt)} = \frac{1}{\mu_r}\iint_{\Delta}\left(\mathbf{W}_{tm}\cdot\mathbf{W}_{tn}\right)ds \tag{24}$$

$$\mathrm{T}_{e(tz)} = \frac{1}{\mu_r}\iint_{\Delta}\left(\mathbf{W}_{tm}\cdot\nabla\alpha_j\right)ds \tag{25}$$

$$\mathrm{T}_{e(zt)} = \frac{1}{\mu_r}\iint_{\Delta}\left(\nabla\alpha_j\cdot\mathbf{W}_{tn}\right)ds \tag{26}$$

$$\mathrm{T}_{e(zz)} = \frac{1}{\mu_r}\iint_{\Delta}\left(\nabla\alpha_i\cdot\nabla\alpha_j\right)ds - k_0^2\varepsilon_r\iint_{\Delta}\alpha_i\alpha_j\,ds \tag{27}$$

The final generalized eigenvalue problem can be obtained by assembling the above element matrices over all the triangular elements in the structure.

$$\begin{bmatrix} S_{tt} & 0 \\ 0 & 0 \end{bmatrix}\begin{bmatrix} E_t \\ E_z \end{bmatrix} = -\gamma^2\begin{bmatrix} \mathrm{T}_{tt} & \mathrm{T}_{tz} \\ \mathrm{T}_{zt} & \mathrm{T}_{zz} \end{bmatrix}\begin{bmatrix} E_t \\ E_z \end{bmatrix} \tag{28}$$

Solving the previous equations yields the propagation constants γ or the eigenvalues. The effective refractive index n_{eff} is obtained by using the relation[14]:

$$n_{eff} = \frac{\gamma}{k_o} \tag{29}$$

3. NONLINEAR AND DISPERSION CHARACTERIZATION

The chromatic dispersion $D(\lambda)$ is calculated from the effective index n_{eff} values versus the wavelength λ by the following expression[15].

$$D(\lambda) = -\frac{\lambda}{c}\frac{\partial^2 \mathrm{Re}\left(n_{eff}(\lambda)\right)}{\partial\lambda^2} \tag{30}$$

Where c is the speed of light in vacuum and $\mathrm{Re}(n_{\mathrm{eff}})$ is the real part of the fundamental mode effective index. The fiber dispersion effects are mathematically realized by using a Taylor series expansion for the propagation constant with respect to the centre frequency ω_0 of the pulse as:

$$\beta(\omega) = \frac{n_{eff}\,\omega}{c} = \beta_0 + \beta_1(\omega-\omega_0) + \frac{1}{2}\beta_2(\omega-\omega_0)^2 + \frac{1}{6}\beta_3(\omega-\omega_0)^3 + \ldots \tag{31}$$

and

$$\beta_m(\omega_0) = \left(\frac{d^m\beta}{d\omega^m}\right)_{\omega=\omega_0} \tag{32}$$

Here $\beta_1 = 1/v_g$ indicates that the pulse envelope moves at group velocity v_g, while β_2 is the group velocity dispersion GVD which is important for broadening the pulse. β_3 represents the third order dispersion. The group velocity dispersion is written as the dispersion parameter[16]:

$$D\left[\,ps/(nm.km)\right] = \frac{d\beta_1}{d\lambda} = -\frac{2\pi c}{\lambda^2}\beta_2 = -\frac{\lambda}{c}\frac{d^2n}{d\lambda^2} \tag{33}$$

The sign of the GVD parameter governs the behaviours of nonlinear effects in optical fibers. If the sign of GVD is positive (D < 0), a normal dispersion regime is occurred where the blue components of the pulse travel slower than the red components, i.e. positive chirp. In contrast, if the sign of GVD is negative (D > 0), an abnormal dispersion regime is occurred where the blue components of the pulse travel faster than the red components, i.e. negative chirp. The last case is the zero-dispersion wavelength (ZDW) when D = 0, where the pulse keeps its original shape and the pulse frequency components travel at the same speed.

Another important parameter is the effective mode area which represents the effective area of the propagating mode in the W-type index fiber. The effective mode area equation is given by[16]:

$$A_{eff} = \frac{\left(\int\int_{-\infty}^{+\infty} |\mathbf{E}(x,y)|^2 \, dxdy\right)^2}{\int\int_{-\infty}^{+\infty} |\mathbf{E}(x,y)|^4 \, dxdy} \tag{34}$$

Here **E**(x,y) is the optical field distribution across the fiber cross-section which is evaluated from the FEM solution of Eqs. (6) and (7.) Then, the effective mode area can be numerically evaluated from Eq. (34). The nonlinear parameter can be expressed as:

$$\gamma\left(W^{-1}m^{-1}\right) = \frac{2\pi n_{NL}}{\lambda A_{eff}} \tag{35}$$

From Eq. (35), the nonlinearity coefficient γ can be controlled via two factors: nonlinear refractive index (n_{NL}) and A_{eff}.

3. DESIGN OF THE W-TYPE INDEX CHALCOGENIDE FIBER

A W-type fiber consists of three different refractive index materials. The core has the largest refractive index of the three, and the inner cladding index is the lowest. Our proposed fiber is composed of core $Ge_{15}Sb_{15}Se_{70}$ (n_1), inner cladding $Ge_{20}Se_{80}$ (n_2) and outer cladding $Ge_{20}Sb_5Se_{75}$ (n_3) as shown in Figure 2, r_1 and r_2 are the core and inner cladding radius, respectively. The wavelength-dependent linear refractive indices of chalcogenide $Ge_{15}Sb_{15}Se_{70}$, $Ge_{20}Se_{80}$ and $Ge_{20}Sb_5Se_{75}$ are obtained from[17,18] and shown in Figure 3.

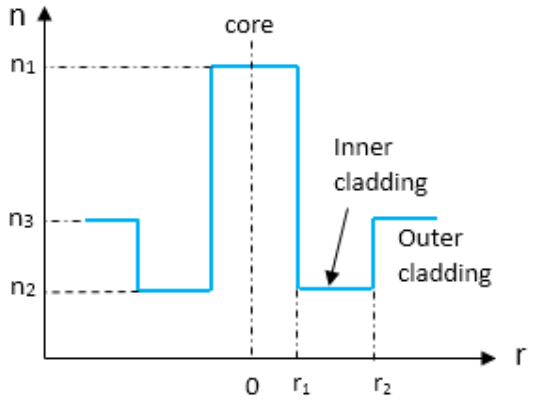

Figure 2. Refractive index profile of a W-type index chalcogenide fiber.

The V-parameter for the W-type index chalcogenide fiber can be written as[7]

$$V = \frac{2\pi r_1}{\lambda} \times NA = \frac{2\pi r_1}{\lambda}\sqrt{n_1^2 - n_3^2} \tag{36}$$

Where λ is the wavelength, and n_1 and n_3 denote the refractive index of the core and outer cladding, respectively. The W-type index has a larger core area for a single-mode operation due to its higher V-parameter (V = 3.8) compared to the

conventional SIF. The advantage of a larger core diameter is the reduction of the coupling losses while still operating under the single-mode condition. However, a smaller effective refractive index of the core and inner cladding may lead to a leakage of the mode power into the outer cladding and therefore result in a catastrophic loss for the mode. This effect can occur when the mode field radius and the operating wavelength become too large. Hence, an effective cut-off wavelength λ_f exists and it occurs at a V-parameter of around 1.4[7]. From the two conditions described above, the operating wavelength must be between λ_f and the single-mode cutoff wavelength (λ_c), that is, $\lambda_c < \lambda < \lambda_f$. In our chalcogenide fiber, we optimize the core diameter to achieve the two above conditions in the range of operating wavelengths between 4.8 and 12µm. The calculation of V-parameter using Eq (36) is shown in Figure 4. The results show that a core diameter of 6 µm is suitable to keep the fiber under the single-mode boundary in the chosen range.

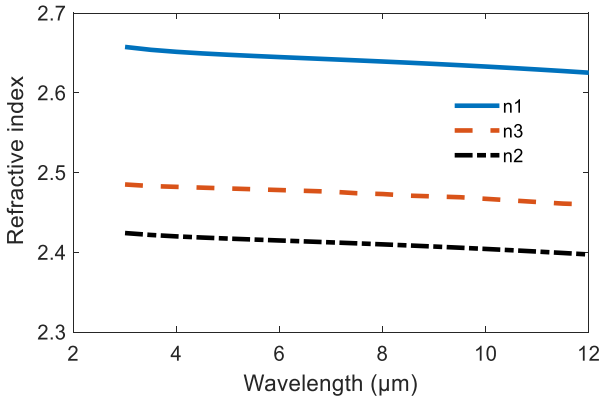

Figure 3. The refractive index for the core, inner and outer cladding versus wavelength for synthesized $Ge_{15}Sb_{15}Se_{70}$, $Ge_{20}Se_{80}$ and $Ge_{20}Sb_5Se_{75}$ glasses.

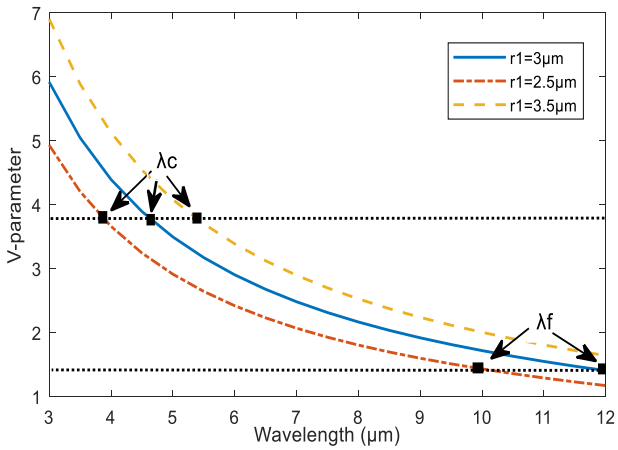

Figure 4. Calculated V-parameter for the W-type index chalcogenide fiber at core radiuses of 2.5µm, 3µm and 3.5µm with single-mode cutoff-wavelengths at λ_c, and cutoff-wavelengths due to leakage losses at λ_f. The single-mode boundary at V = 3.8 and the leakage boundary at V = 1.4 are marked with black dotted lines.

4. RESULTS AND DISCUSSION

The guiding properties of the designed W-type index fiber are analyzed by calculating the guided modes using our FEM software tool. Several meshes with different polynomial approximations are tested to ensure that the error induced by the spatial discretisation does not have a sizeable influence on the computed modes.

Figure 5 illustrates the chromatic dispersion characteristic of our reported fiber structure with a core diameter of 6µm and different inner cladding diameters. As shown in Figure 5, there are two zero-dispersion wavelengths (ZDWs) per curve. The first ZDWs remains nearly fixed, at around 4.3µm, for different inner cladding diameters. The second ZDWs increases with the inner cladding diameter. For an inner cladding diameter of 9µm, 12µm and 18µm the second ZDWs

are located at 6µm, 6.5µm and 7µm respectively. Between these two ZDWs the fiber exhibits a low and flat anomalous dispersion. Moreover, the proposed fiber structure shifts ZDWs to longer wavelengths with a smaller core diameter size than in the case of SIF. Higher order dispersion values (β_2 - β_{10}) of the W-type index chalcogenide for the pump wavelength at 6.3 µm are listed in Table 1.

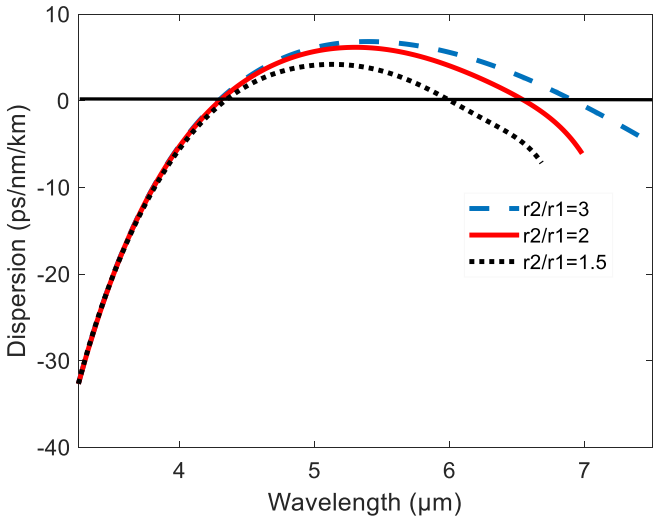

Figure 5. Calculated dispersion profiles versus wavelength for the W-type index chalcogenide fiber.

Table 1. Higher order dispersion values of the W-type index chalcogenide for the pump wavelength at 6.3 µm.

β_n	Value
β_2(ps^2/m)	-2.6
β_3(ps^3/m)	1.3×10^{-3}
β_4(ps^4/m)	3.55×10^{-7}
β_5(ps^5/m)	1.51×10^{-9}
β_6(ps^6/m)	1.79×10^{-11}
β_7(ps^7/m)	-0.063×10^{-12}
β_8(ps^8/m)	-0.00138×10^{-14}
β_9(ps^9/m)	9.7×10^{-20}
β_{10}(ps^{10}/m)	-1.2×10^{-23}

The calculated spectral variation of the effective mode area is shown in Figure 6. It is clearly observed that the effective mode area increases with the inner cladding. From the above simulation, we select the inner cladding diameter of 12 µm (r_2/r_1=2), and a pump wavelength of 6.3µm, which is near the second ZDWs in the anomalous dispersion regime. At this pump wavelength, the dispersion is D =3.24ps/(nm·km) and the effective area equals 32 µm^2. Typically, the $Ge_{15}Sb_{15}Se_{70}$ glass offers a high nonlinear refractive index (n_{NL}) of about 10.34 m^{2}W^{-1} at the wavelength of 1.55 µm[19].

An efficient way to achieve wide Mid-IR SC generation is to pump the nonlinear fiber in its anomalous dispersion regime. At this regime, the pulse spectrum is broadened through soliton effects. The numerically calculated value of nonlinear parameter is about 0.1225 $W^{-1} m^{-1}$ at the pump wavelength of 6.3 µm which is twice time higher than previously reported step-index fiber[20]. As a result, the proposed W-type index chalcogenide structure ensures single-mode propagation, which improves the nonlinearity, a flattened dispersion profile and low losses due to a tight confinement of the mode within the core.

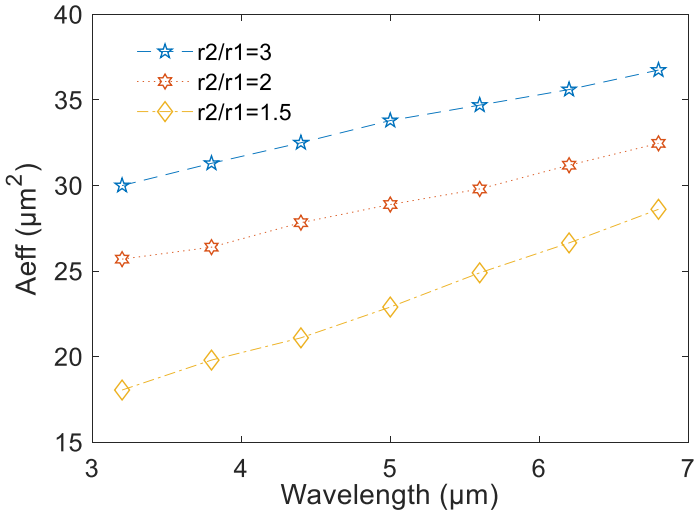

Figure 6. Effective area versus wavelength (µm) for the W-type index chalcogenide fiber at different inner cladding diameters.

5. CONCLUSION

In summary, this paper presents a design of a robust W-type index chalcogenide fiber for Mid-IR SC beyond 10µm. Our fiber design consists of $Ge_{15}Sb_{15}Se_{70}$ glass core, $Ge_{20}Se_{80}$ glass inner cladding and $Ge_{20}Sb_5Se_{75}$ glass outer cladding. The optical mode distribution of the chalcogenide fiber is simulated by a finite element method based on edge elements. With 6-µm core diameter and 12-µm inner cladding diameter, the proposed fiber design exhibits flat anomalous dispersion in the wavelength range (4.3-6.5µm) with a peak of about 7ps/(nm·km). The position of the second ZDW can be easily and precisely controlled by the inner cladding size. The larger the inner cladding diameter, the longer will be the zero-dispersion wavelength. However, the increase of the inner cladding diameter leads also to an increase of the effective mode area and therefore a smaller fiber nonlinear coefficient. The proposed design is more suitable for a pump wavelength at 6.3µm which is located between two ZDWs.

Funding Information. This work was supported by the High Committee for Education Development in Iraq (HCED).

REFERENCES

[1] Cruz, F. C., Maser, D. L., Johnson, T., Yeas, G., Klose, A., Giorgetta, F. R., Coddington, I., and Diddams, S. A., "Mid-infrared optical frequency combs based on difference frequency generation for molecular spectroscopy," Opt. Express 23(20), 26814–26824 (2015).

[2] Schliesser, A., Picqué, N., and Hänsch, T. W., "Mid-infrared frequency combs," Nat. Photonics 6(7), 440–449 (2012).

[3] Swiderski, J., "High-power mid-infrared supercontinuum sources: Current status and future perspectives," Prog. Quantum Electron. 38, 189–235 (2014).

[4] Nagasaka, K., Liu, L., Tuan, T. H., Cheng, T., Matsumoto, M., Tezuka, H., … Ohishi, Y., "Numerical investigation of highly coherent mid-infrared supercontinuum generation in chalcogenide double-clad fiber," Opt. Fiber Technol. 36, 82–91 (2017).

[5] Cheng, T., Nagasaka, K., Tuan, T. H., Xue, X., Matsumoto, M., Tezuka, H., … Ohishi, Y., "Mid-infrared supercontinuum generation spanning 2 to 15 μm in a chalcogenide step-index fiber," Opt. Lett. 41, 2117 (2016).
[6] Brilland, L., Smektala, F., Renversez, G., Chartier, T., Troles, J., Nguyen, T., … Monteville, A., "Fabrication of complex structures of Holey Fibers in Chalcogenide glass," Opt. Express 14, 1280-1285 (2006).
[7] Kedenburg, S., Steinle, T., Mörz, F., Steinmann, A., Nguyen, D., Rhonehouse, D., … Giessen, H., "Solitonic supercontinuum of femtosecond mid-IR pulses in W-type index tellurite fibers with two zero dispersion wavelengths," APL Photonics 1, 86101, (2016).
[8] Wei, C., Zhu, X., Norwood, R. A., Song, F., and Peyghambarian, N., "Numerical investigation on high power mid-infrared supercontinuum fiber lasers pumped at 3 μm," Opt. Express 21, 29488-29504 (2013).
[9] Klocek, P. and Colombo, L., 'Index of refraction, dispersion, bandgap and light scattering in GeSe and GeSbSe glasses', Journal of Non-Crystalline Solids 93, 1–16 (1987).
[10] Ou, H., Dai, S., Zhang, P., Liu, Z., Wang, X., Chen, F., … Wang, R., "Ultrabroad supercontinuum generated from a highly nonlinear Ge–Sb–Se fiber," Opt. Lett. 41, 3201 (2016).
[11] Pelosi, G., Coccioli, R., and Selleri, S., "Microwave Guidance Structure: characterization" in [Quick Finite Elements for Electromagnetic Waves 2nd edition] ARTECH HOUSE, pp.59-82, (2009).
[12] Jin, J., [The Finite Element Method in Electromagnetics], J. Wiley & Sons (2002).
[13] Reddy, C. J., Deshpande, M. D., Cockrell, C. R., & Beck, F. B., "Finite element method for eigenvalue problems in electromagnetics," NASA Technical Paper, 3485, (1994).
[14] Jamatia, P., Saini, T. S., Kumar, A., and Sinha, R. K., "Design and analysis of a highly nonlinear composite photonic crystal fiber for supercontinuum generation: visible to mid-infrared," Appl. Opt. 55, 6775 (2016).
[15] Butterworth, J. H., Jayasuriya, D., Li, Q. Q., Furniss, D., Moneim, N. A., Barney, E., … Seddon, A. B., "Towards mid-infrared supercontinuum generation: Ge-Sb-Se mid-infrared step-index small-core optical fiber," SPIE BIOS 8938, 89380 (2014).
[16] Agrawal, G. P, [Application of Nonlinear Fiber Optics, 2nd edition], Academic press, (2001).
[17] Petersen, C. R., Møller, U., Kubat, I., Zhou, B., Dupont, S., Ramsay, J., … Bang, O., "Mid-infrared supercontinuum covering the 1.4–13.3 μm molecular fingerprint region using ultra-high NA chalcogenide step-index fibre" Nat. Photon. 8, 830 (2014).
[18] Chen, L., Chen, F., Dai, S., Tao, G., Yan, L., Shen, X., … Xu, Y., "Third-order nonlinearity in Ge-Sb-Se glasses at mid-infrared wavelengths," Mater. Res. Bull. 70, 204–208 (2015).
[19] Wang, T., Gai, X., Wei, W., Wang, R., Yang, Z., Shen, X., … Luther-Davies, B., "Systematic z-scan measurements of the third order nonlinearity of chalcogenide glasses," Opt. Mater. Exp. 4, 1011 (2014).
[20] Møller, U., Yu, Y., Kubat, I., Petersen, C. R., Gai, X., Brilland, L., … Bang, O., "Multi-milliwatt mid-infrared supercontinuum generation in a suspended core chalcogenide fiber," Opt. Exp. 23, 3282-3291 (2015).